JAM CM Journal of Applied Mathematics and Computational Mechanics 2024, 23(4), 42-55
www.amcm.pcz.pl p-ISSN 2299-9965
DOI: 10.17512/jamcm.2024.4.04 e-ISSN 2353-0588

INVESTIGATION OF THE STOCHASTICALLY DEFECTIVE PLATES WITH STRENGTH ANISOTROPY LIMIT STATE

Roman Kvit

Department of Mathematics, Lviv Polytechnic National University
Lviv, Ukraine
kvit_rom@ukr.net

Received: 17 September 2024; Accepted: 20 November 2024

Abstract. The algorithm for finding the probability of failure of stochastically defective plates in a flat stress field based on a certain idea about structural rearrangement due to technological deformation processing (extraction) is considered. The plate is isotropic before technological processing, in which defects-cracks, which do not interact with each other, are evenly distributed. Cracks are characterized by the length and angle of orientation relative to the extraction direction, which are statistically independent random variables. The relationship for the failure loading integral probability distribution function of plates with extraction was obtained. The probability of plate failure with strength anisotropy was investigated.

MSC 2010: *74R10, 74R99, 60K35, 82C03*
Keywords: *crack, technological deformation treatment, stochasticity, probability of failure, integral probability distribution function, extraction coefficient*

1. Introduction

Some types of technological deformation treatment of materials lead to changes in the geometric parameters of defects and their structure. Although the level of physical and chemical connections between the microparticles of the material remains practically unchanged, the macroscopic strength and probability of failure of the bodies after such treatments can change significantly. For example, materials subjected to directional plastic deformation during processing acquire properties of strength anisotropy [1, 2], which can be explained by the appearance of a certain texture (predominant orientation) of defects. In the article [3], a study of the scale effect of the structural materials failure is carried out. The paper [4] proposes an algorithm of probabilistic fracture mechanics for assessing the reliability of structural elements with crack-type defects, which takes into account uncertainties in structural analysis. A solution to the problem of brittle failure mechanics was obtained [5], considering the random distribution of microcracks in terms of shape, spatial arrangement, and orientation. The paper [6] describes an integrated model

for analyzing the reliability of a continuous structure. The work [7] considers the criterion of quasi-brittle fracture, which is based on local values related to the energy release rate. A statistical approach to assessing the strength of materials at brittle fracture, taking into account the scale effect, is considered in [8]. The process of assessing the probability of failure of composite structural materials under the conditions of working loading is complicated by non-homogeneous mechanical properties that arise in the process of their manufacture [9]. The analytical model for calculating the probability of failure of composite material samples is considered in [10]. In the article [11], a probabilistic approach is proposed for assessing the reliability of unidirectional carbon fiber-reinforced composite materials under biaxial loading. A method of researching the tensile strength of brittle materials is proposed in [12]. A method of calculating the probability of failure under mechanical loading conditions has been developed [13]. In article [14], an assessment of the welded steel joints probability of failure containing surface defects was carried out.

In this article, based on a certain idea about the structural rearrangement due to the technological deformation treatment (extraction) of stochastically defective plates, the probability of failure is determined, and the reliance of the material strength anisotropy acquired during treatment on the extraction coefficient and the number of defects was investigated.

2. Formulation of the problem

Let's investigate the structural anisotropy of the material, which occurs during technological extraction. Consider a plate that is isotropic before technological processing, in which defects-cracks that do not interact with each other are evenly distributed. Cracks are characterized by the length $2l_*$ and angle of orientation α_* relative to the extraction direction. The indicated parameters are statistically independent random variables. Assuming the isotropic nature of the plate material, the probability distribution density will be set by the uniform law [15] $f^{(1)}(\alpha_*) = 1/\pi$ $\left(\alpha \in (-\pi/2; \pi/2)\right)$.

In work [15], the probability distribution density of l_* was chosen as a linearly decreasing distribution $f^{(2)}(l_*) = 2\left(1 - l_*/c_*\right)/c_*$ $(0 \le l_* \le c_*)$, c_* is a finite structural characteristic. We choose the probability distribution density of l_* in the form of a generalized β-distribution $f^{(2)}(l_*) = (r+1)\left(1 - l_*/c_*\right)^r / c_*$, $r \ge 0$ [16]. The integral distribution function is written as $F^{(2)}(l_*) = 1 - \left(1 - l_*/c_*\right)^{r+1}$. The parameter r reflects the following property: the longer the defect, the lower the probability of its occurrence in the material. Experimental data [17, 18] also indicate the nature of the density of the probability distribution of crack sizes.

Then, the density of the compatible probability distribution of α_* and l_*

$$f^{(1)}(\alpha_*, l_*) = (r+1)\left(1 - l_*/c_*\right)^r / (\pi c_*). \tag{1}$$

The material of the plate in a softened state is subjected to technological deformation treatment (extraction) with a coefficient $m \geq 1$, which shows how many times the size of the material elements increases in the direction of extraction, and then hardens (becomes brittle). The values of extraction coefficients for certain lamellar materials are chosen according to the reference [19].

We assume that the cracks during extraction behave like flexible tensile threads and the material is incompressible. This means that when the length of a fixed element of an object increases by a factor of m, and its width and thickness decrease by a factor of $\sqrt{m}$. Correspondingly, there are changes in the structure of the material cracking, that is, the orientation and length of the cracks change.

For geometric reasons, we establish a relationship between the parameters of the cracks before and after extraction:

$$l = l_* \sqrt{m^{-1} \sin^2 \alpha_* + m^2 \cos^2 \alpha_*}; \tag{2}$$

$$\alpha = \operatorname{arctg}\left(\operatorname{tg} \alpha_* \big/ m^{3/2} \right). \tag{3}$$

From relations (2)-(3), we obtain the following inverse relationship:

$$l_* = l m^{-1} \sqrt{m^3 \sin^2 \alpha + \cos^2 \alpha}; \tag{4}$$

$$\alpha_* = \operatorname{arctg}\left(m^{3/2} \operatorname{tg} \alpha \right). \tag{5}$$

3. Probability distribution densities of the defect's geometric random parameters after technological deformation treatment

Let's find the probability distribution densities of α and l $(0 \leq l \leq c)$, that are changed as a result of technological deformation treatment. The relationship between structural parameters c and c_* according to expression (2), establishes the expression

$$c = c_* \sqrt{m^{-1} \sin^2 \alpha_* + m^2 \cos^2 \alpha_*}.$$

According to [20]

$$f^{(2)}(\alpha, l) = f^{(1)}(\alpha_*, l_*) \left(\frac{\partial \alpha_*}{\partial \alpha} \frac{\partial l_*}{\partial l} - \frac{\partial l_*}{\partial \alpha} \frac{\partial \alpha_*}{\partial l} \right). \tag{6}$$

By substituting expressions (1), (4), and (5) into formula (6), we obtain

$$\begin{aligned} & f^{(2)}(\alpha, l) = \frac{(r+1)\sqrt{m}}{\pi c} \left(1 - \frac{l \psi(\alpha, m)}{mc} \right)^r \psi^{-1}(\alpha, m), \\ & -\pi/2 \leq \alpha \leq \pi/2, \;\; 0 \leq l \leq cm\psi^{-1}(\alpha, m), \;\; \psi(\alpha, m) = \sqrt{m^3 \sin^2 \alpha + \cos^2 \alpha}. \end{aligned} \tag{7}$$

The indicated parameter change interval l ensures the condition of non-negativity of the density of the compatible probability distribution (7). With the value of the parameter $r = 1$, we have the partial case [15].

Using (7), we obtain the probability distribution densities after extraction

$$f^{(1)}(\alpha) = \frac{(r+1)\sqrt{m}}{\pi c \psi(\alpha, m)} \int_0^{cm\psi^{-1}(\alpha,m)} \left(1 - \frac{l\psi(\alpha, m)}{mc}\right)^r dl. \tag{8}$$

$$f^{(2)}(l) = \frac{2(r+1)\sqrt{m}}{\pi c} \int_0^{\pi/2} \left(1 - \frac{l\psi(\alpha, m)}{mc}\right)^r \psi^{-1}(\alpha, m)\, d\alpha. \tag{9}$$

In particular $r = 1$, from formula (8), we analytically obtain the expression [21]

$$f^{(1)}(\alpha) = \frac{2\sqrt{m}}{\pi c \psi(\alpha, m)} \int_0^{cm\psi^{-1}(\alpha,m)} \left(1 - \frac{l\psi(\alpha, m)}{mc}\right) dl = \frac{m^{3/2}}{\pi(m^3 \sin^2\alpha + \cos^2\alpha)}. \tag{10}$$

Distributions (7)-(10) explicitly contain the coefficient of technological extraction m. With its help, you can control the structural, and therefore the strength properties of the material. According to (10), the most probable value of the orientation of the cracks $Mo(\alpha) = 0$, i.e., the greatest probability of placement of cracks is in the direction of the technological extraction. In the extraction direction, the presence of the longest defects is more likely. With the increase of the extraction, this process of structural reconstruction intensifies.

4. The failure loading probability distribution function

Let the plate of thickness H and area S be subjected to biaxial tension, compression, or tension-compression in two mutually perpendicular directions by a uniform loading P and $Q = \eta P$. For plates with a directional structure of defects, in contrast to isotropic materials [22], the angle of the action direction of applied loading with the direction of calculation of defect orientation, which coincides with the direction of technological extraction of the material, is important. The direction of the loading P coincides with the direction of the preliminary extraction.

The failure loading probability distribution function of a plate element with one crack is recorded according to the formula to determine the probability distribution of the function from random variables [15]

$$F_1(P, \eta) = \iint\limits_{K_{Ic}(\pi l)^{-1/2} \varphi(\alpha,\eta) < P} f^{(2)}(\alpha, l)\, d\alpha\, dl, \quad P_{\min} \le P < \infty, \tag{11}$$

where the function $\varphi(\alpha, \eta)$ is represented by various analytical expressions [23], based on the criterion for calculating the ultimate stresses from the condition of

$$\varphi(\alpha,\eta)=\begin{cases}(\sin^2\alpha+\eta^2\cos^2\alpha)^{-1/2}, & \sigma_n\geq 0,\\ 2\left((1-\eta)\sin 2\,|\,\alpha\,|\right)^{-1}, & \sigma_n\leq 0,\end{cases} \tag{12}$$

where σ_n are stresses normal to the crack line.

The values $P_{\min}$ and $P_{\max}$ are random variables and are determined from [23]

$$|\,P\,|=K_{Ic}(\pi l)^{-1/2}\varphi(\alpha,\eta); \tag{13}$$

$$P_{\min}(\eta)=K_{Ic}(\pi c)^{-1/2}\min_{\alpha}\varphi(\alpha,\eta),\quad P_{\max}(\eta)=\infty, \tag{14}$$

where K_{Ic} is the critical stress intensity factor that describes the material's resistance to crack growth, $\varphi(\alpha,\eta)$ is a known function, the form of which depends on the type of defect, the range of values of α and η, the approach to solving the problem of the limited state of the body, etc. The expressions (14) are obtained from (13) as the minimum and maximum value of the failure loading according to two variables α and l.

In expression (11), taking into account (12)-(14), the integration is carried out over those possible variables of α and l for which $K_{Ic}(\pi l)^{-1/2}\varphi(\alpha,\eta)<P$.

Substitute expression (7) in (11):

$$F_1(P,\eta)=\frac{(r+1)\sqrt{m}}{\pi c}\iint\limits_{K_{Ic}(\pi l)^{-1/2}\varphi(\alpha,\eta)<P}\left(1-\frac{l\psi(\alpha,m)}{mc}\right)^{r}\psi^{-1}(\alpha,m)\,d\alpha\,dl. \tag{15}$$

We represent the double integral in formula (15) through the repeated integral

$$F_1(P,\eta)=\frac{(r+1)\sqrt{m}}{\pi c}\int\limits_{\alpha\in\Omega}\left[\int\limits_{\frac{K_{Ic}^2\varphi^2(\alpha,\eta)}{\pi P^2}}^{\frac{cm}{\psi(\alpha,m)}}\left(1-\frac{l\psi(\alpha,m)}{mc}\right)^{r}\psi^{-1}(\alpha,m)\,dl\right]d\alpha. \tag{16}$$

In formula (16), Ω is the area of change of the parameter α from $-\pi/2$ to $\pi/2$, excludes areas in which $K_{Ic}^2(\pi P^2)^{-1}\varphi^2(\alpha,\eta)\geq cm\psi^{-1}(\alpha,m)$.

From expressions (7) and (13), we obtain

$$0\leq K_{Ic}^2(\pi P^2)^{-1}\varphi^2(\alpha,\eta)\leq cm\psi^{-1}(\alpha,m). \tag{17}$$

From formula (17), by notations (7) and (12), we write down the expression

$$P=K_{Ic}\left(m^3\sin^2\alpha+\cos^2\alpha\right)^{1/4}\left(\pi cm(\sin^2\alpha+\eta^2\cos^2\alpha)\right)^{-1/2}. \tag{18}$$

Formula (18) makes it possible to determine the intervals of change of the failure loading under different types of stress states and to calculate certain critical values of the crack orientation angle.

We find $F_1(P,\eta)$ $(P \ge 0, Q \ge 0)$. From relation (18), we get

$$K_{Ic} m^{1/4} (\pi c)^{-1/2} \le P \le K_{Ic} \eta^{-1} (\pi c m)^{-1/2}. \tag{19}$$

From the condition $K_{Ic} m^{1/4} (\pi c)^{-1/2} \le K_{Ic} \eta^{-1} (\pi c m)^{-1/2}$: $0 \le \eta \le m^{-3/4}$. Figure 1a schematically depicts the region of integration in formula (16) for the loading change interval P (19). The curve $l = K_{Ic}^2 \left(\pi P^2 (\sin^2\alpha + \eta^2 \cos^2\alpha) \right)^{-1}$ is marked in olive color, and the curve $l = cm \left(m^3 \sin^2\alpha + \cos^2\alpha \right)^{-1/2}$ is orange.

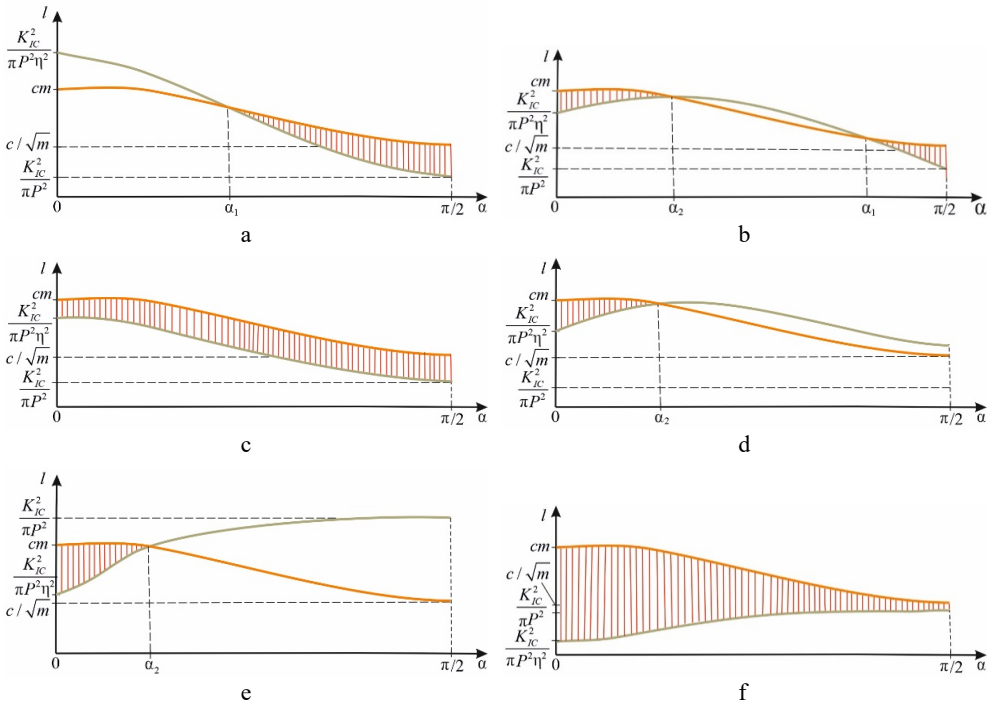

Fig. 1. Region of integration for the function $F_1(P,\eta)$ under biaxial tension $(P \ge 0, Q \ge 0)$

The point of intersection of the marked curves is determined from the system

$$\begin{cases} l = K_{Ic}^2 \pi^{-1} P^{-2} (\sin^2\alpha + \eta^2 \cos^2\alpha)^{-1}; \\ l = cm (m^3 \sin^2\alpha + \cos^2\alpha)^{-1/2}. \end{cases} \tag{20}$$

From (20), we obtain the following values:

$$\alpha_{1,2}=\arcsin\left(\left(\sqrt{2}\,|1-\eta^2|\,cmP^2\right)^{-1}\sqrt{\frac{K_{Ic}^4(m^3-1)}{\pi^2}\pm\frac{K_{Ic}^2\sqrt{T}}{\pi}-2m^2\eta^2\left(1-\eta^2\right)c^2P^4}\right);$$

$$T=K_{Ic}^4\left(m^3-1\right)^2\Big/\pi^2-4m^2\left(m^3\eta^2-1\right)\left(1-\eta^2\right)c^2P^4. \tag{21}$$

In expression (21), the sign "+" corresponds to the α_1, the sign "–" to the α_2.

According to expression (19), consider the loading change interval

$$K_{Ic}\eta^{-1}(\pi cm)^{-1/2}\le P\le K_{Ic}(m^3-1)^{1/2}(2\pi cm)^{-1/2}\left((m^3\eta^2-1)(1-\eta^2)\right)^{-1/4}. \tag{22}$$

The loading change limit $P=K_{Ic}(m^3-1)^{1/2}(2\pi cm)^{-1/2}\left((m^3\eta^2-1)(1-\eta^2)\right)^{-1/4}$ is obtained from the condition $T=0$.

From $K_{Ic}\eta^{-1}(\pi cm)^{-1/2}\le K_{Ic}(m^3-1)^{1/2}(2\pi cm)^{-1/2}\left((m^3\eta^2-1)(1-\eta^2)\right)^{-1/4}$, we get the parameter η change interval: $\left(2/(1+m^3)\right)^{1/2}\le\eta\le m^{-3/4}$. The region of integration in formula (16) for the loading change interval P (22) is shown in Figure 1b.

For $\sqrt{2/(1+m^3)}\le\eta\le m^{-3/4}$, $K_{Ic}(m^3-1)^{1/2}(2\pi cm)^{-1/2}\left((m^3\eta^2-1)(1-\eta^2)\right)^{-1/4}\le P<\infty$, or $0\le\eta\le\sqrt{2/(1+m^3)}$, $K_{Ic}\eta^{-1}(\pi cm)^{-1/2}\le P<\infty$ the region of integration is presented in Figure 1c.

For $m^{-3/4}\le\eta\le 1$, $K_{Ic}m^{1/4}(\pi c)^{-1/2}\le P\le K_{Ic}(m^3-1)^{1/2}(2\pi cm)^{-1/2}\left((m^3\eta^2-1)(1-\eta^2)\right)^{-1/4}$, the region of integration is shown in Figure 1d.

The region of integration in Figure 1b is shown for $m^{-3/4}\le\eta\le\sqrt{(1+m^3)/(2m^3)}$, $K_{Ic}m^{1/4}(\pi c)^{-1/2}\le P\le K_{Ic}(m^3-1)^{1/2}(2\pi cm)^{-1/2}\left((m^3\eta^2-1)(1-\eta^2)\right)^{-1/4}$. The region of integration is presented in Figure 1c when $m^{-3/4}\le\eta\le\sqrt{(1+m^3)/(2m^3)}$, $K_{Ic}(m^3-1)^{1/2}(2\pi cm)^{-1/2}\left((m^3\eta^2-1)(1-\eta^2)\right)^{-1/4}\le P<\infty$, or $\sqrt{(1+m^3)/(2m^3)}\le\eta\le 1$, $K_{Ic}m^{1/4}(\pi c)^{-1/2}\le P<\infty$.

Let's consider the case $1\le\eta<\infty$. When $K_{Ic}\eta^{-1}(\pi cm)^{-1/2}\le P\le K_{Ic}m^{1/4}(\pi c)^{-1/2}$ the region of integration is in Figure 1e, for $K_{Ic}m^{1/4}(\pi c)^{-1/2}\le P<\infty$ in Figure 1f.

We find $F_1(P,\eta)$ $(P\ge 0, Q\le 0)$. The function $\varphi(\alpha,\eta)$ (12)

$$\varphi(\alpha,\eta)=\begin{cases}2\left((1-\eta)\sin 2\,|\,\alpha\,|\right)^{-1},\ 0\le|\,\alpha\,|\le\operatorname{arctg}\sqrt{|\,\eta\,|};\\ \left(\sin^2\alpha+\eta^2\cos^2\alpha\right)^{-1/2},\ \operatorname{arctg}\sqrt{|\,\eta\,|}\le|\,\alpha\,|\le\pi/2.\end{cases} \tag{23}$$

Let's consider the case $-1 \le \eta < 0 \left(|Q| \le P\right)$. We take into account expression (23). When $K_{Ic}|\eta|^{-1}(\pi cm)^{-1/2}(1-m^3\eta)^{1/4}(1-\eta)^{-1/4} \le P \le K_{Ic} m^{1/4}(\pi c)^{-1/2}$ and $(1-m^3\eta)^{1/3}\left((1-\eta)\eta^2\right)^{-1/3} \le m$, the region of integration is in Figure 2a. In this figure and the following ones, the curve $l = 4K_{Ic}^2\left(\pi P^2(1-\eta)^2\sin^2 2\alpha\right)^{-1}$ is marked in a sea green color. The left limit of the loading change interval P is the solution of the equation $4K_{Ic}^2\left(\pi P^2(1-\eta^2)\sin^2 2\alpha_3\right)^{-1} = mc\left(k^3\sin^2\alpha_3 + \cos^2\alpha_3\right)^{-1/2}$.

The inequality $\left(1-m^3\eta\right)^{1/3}\left((1-\eta)\eta^2\right)^{-1/3} \le m$ is obtained from $P_{\min} \le P_{\max}$.

The coordinate α_4 (Fig. 2a) is the solution of the equation

$$\cos^4 2\alpha - 2\cos^2 2\alpha - \frac{8K_{Ic}^4(1-m^3)\cos 2\alpha}{\pi^2 m^2(1-\eta)^4 c^2 P^4}\left((1-m^3)\cos 2\alpha + 1 + m^3\right) + 1 = 0, \quad (24)$$

and satisfies the condition $0 \le \alpha_4 \le \alpha_3$.

For $-1 \le \eta < 0 \left(|Q| \le P\right)$, at $K_{Ic} m^{1/4}(\pi c)^{-1/2} \le P < \infty$ and $\left(1-m^3\eta\right)^{1/3}\left((1-\eta)\eta^2\right)^{-1/3} \ge m$ the region of integration is shown in Figure 2b.

Consider the case $-1 < \eta \le 0$, $\left(1-m^3\eta\right)^{1/3}\left((1-\eta)\eta^2\right)^{-1/3} \ge m$. When $K_{Ic} m^{1/4}(\pi c)^{-1/2} \le P \le K_{Ic}|\eta|^{-1}(\pi cm)^{-1/2}\left(1-m^3\eta\right)^{1/4}(1-\eta)^{-1/4}$ the region of integration is in Figure 2c. For $2K_{Ic}(1-\eta)^{-1}(\pi cm)^{-1/2}\left(0.5(1+m^3)\right)^{1/4} \le P < \infty$ in Figure 2b.

Consider the loading ratio interval $-\infty < \eta \le 1 \left(|Q| \ge P\right)$. Then $\alpha_3 \ge \pi/4$ and the sea green curve takes a minimum value at the point $\alpha = \pi/4$. We equate the functions describing the curves $l = cm\left(m^3\sin^2\alpha + \cos^2\alpha\right)^{-1/2}$ and $l = 4K_{Ic}^2\left(\pi P^2(1-\eta)^2\sin^2 2\alpha\right)^{-1}$, at $\alpha = \pi/4$

$$\sqrt{2}\, cm\left(m^3+1\right)^{-1/2} = 4K_{Ic}^2\left(\pi P^2(1-\eta)^2\right)^{-1}. \quad (25)$$

From the expression (25), we get $P = 2K_{Ic}(1-\eta)^{-1}(\pi cm)^{-1/2}\left(0.5(1+m^3)\right)^{1/4}$. For $2K_{Ic}(1-\eta)^{-1}(\pi cm)^{-1/2}\left(0.5(1+m^3)\right)^{1/4} \le P \le K_{Ic}|\eta|^{-1}(\pi cm)^{-1/2}\left(1-m^3\eta\right)^{1/4}(1-\eta)^{-1/4}$ we get the region of integration in Figure 2d, where α_3, α_5 are solutions of equation (24), respectively, on the intervals $(0;\pi/4)$ and $(\pi/4;\alpha_3)$.

For $K_{Ic}|\eta|^{-1}(\pi cm)^{-1/2}\left(1-m^3\eta\right)^{1/4}(1-\eta)^{-1/4} \le P \le K_{Ic} m^{1/4}(\pi c)^{-1/2}$, we get the region of integration in Figure 2e, for $K_{Ic} m^{1/4}(\pi c)^{-1/2} \le P < \infty$ in Figure 2f.

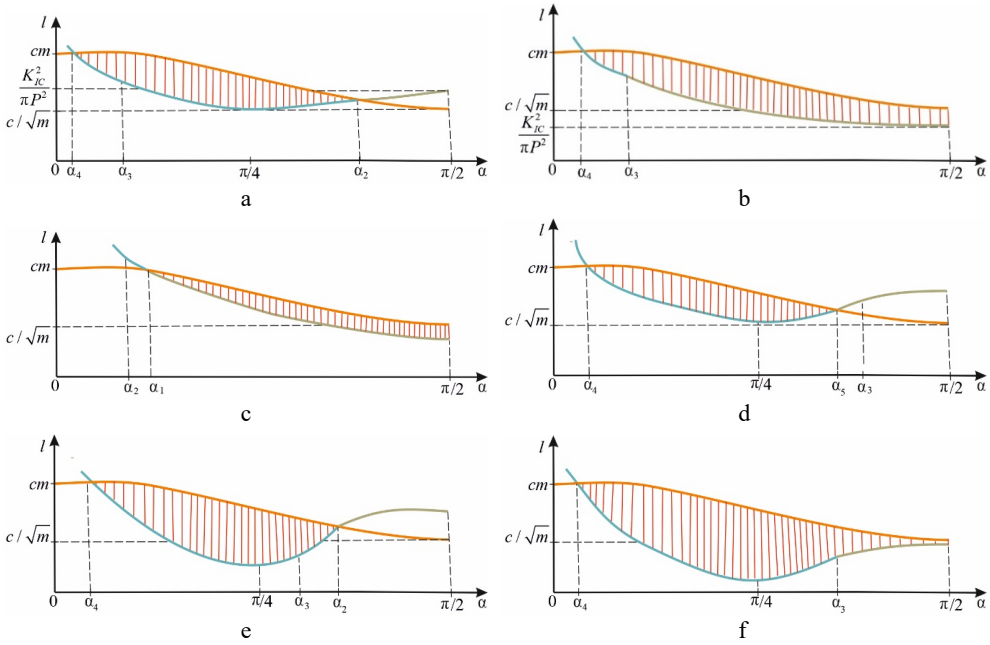

Fig. 2. Region of integration for the function $F_1(P,\eta)$ under tension-compression $(P \ge 0, Q \le 0)$

Consider the case of compression-tension of plates $(P \le 0, Q \ge 0)$. Then

$$\varphi(\alpha,\eta) = \begin{cases} (\sin^2\alpha + \eta^2\cos^2\alpha)^{-1/2}, \ 0 \le |\alpha| \le \operatorname{arctg}\sqrt{|\eta|}; \\ 2\big((1-\eta)\sin 2|\alpha|\big)^{-1}, \ \operatorname{arctg}\sqrt{|\eta|} \le |\alpha| \le \pi/2. \end{cases} \tag{26}$$

Consider the loading ratio interval $-\infty < \eta \le -1 \ (Q \ge |P|, \alpha_3 \ge \pi/4)$. We take into account expression (26). When $K_{Ic}|\eta|^{-1}(\pi cm)^{-1/2} \le -P \le K_{Ic}|\eta|^{-1}(\pi cm)^{-1/2}\left(1-m^3\eta\right)^{1/4}(1-\eta)^{-1/4}$, the region of integration is shown in Figure 3a, for $K_{Ic}|\eta|^{-1}(\pi cm)^{-1/2}\left(1-m^3\eta\right)^{1/4}(1-\eta)^{-1/4} \le -P < \infty$ in Figure 3b, where α_5 is the solution of equation (25) on the interval $(\alpha_3;\pi/2)$.

Consider the conditions $-1 < \eta \le 0 \ (Q < |P|, \alpha_3 < \pi/4)$ and $|\eta| \le \sqrt{(1-\eta)/(1-m^3\eta)}$. The region of integration is shown in Figure 3c for $2K_{Ic}(1-\eta)^{-1}(\pi cm)^{-1/2}\left(0.5(1+m^3)\right)^{1/4} \le -P \le K_{Ic}|\eta|^{-1}(\pi cm)^{-1/2}\left(1-m^3\eta\right)^{1/4}(1-\eta)^{-1/4}$, where α_4, α_5 are the solutions of equation (26), respectively, on the intervals $(\alpha_3;\pi/4)$ and $(\pi/4;\pi/2)$. We get the region of integration in Figure 3d for $K_{Ic}|\eta|^{-1}(\pi cm)^{-1/2}\left(1-m^3\eta\right)^{1/4}(1-\eta)^{-1/4} \le -P \le K_{Ic}|\eta|^{-1}(\pi cm)^{-1/2}$. Here α_5 is the solution of equation (26) on the interval $(\pi/4;\pi/2)$.

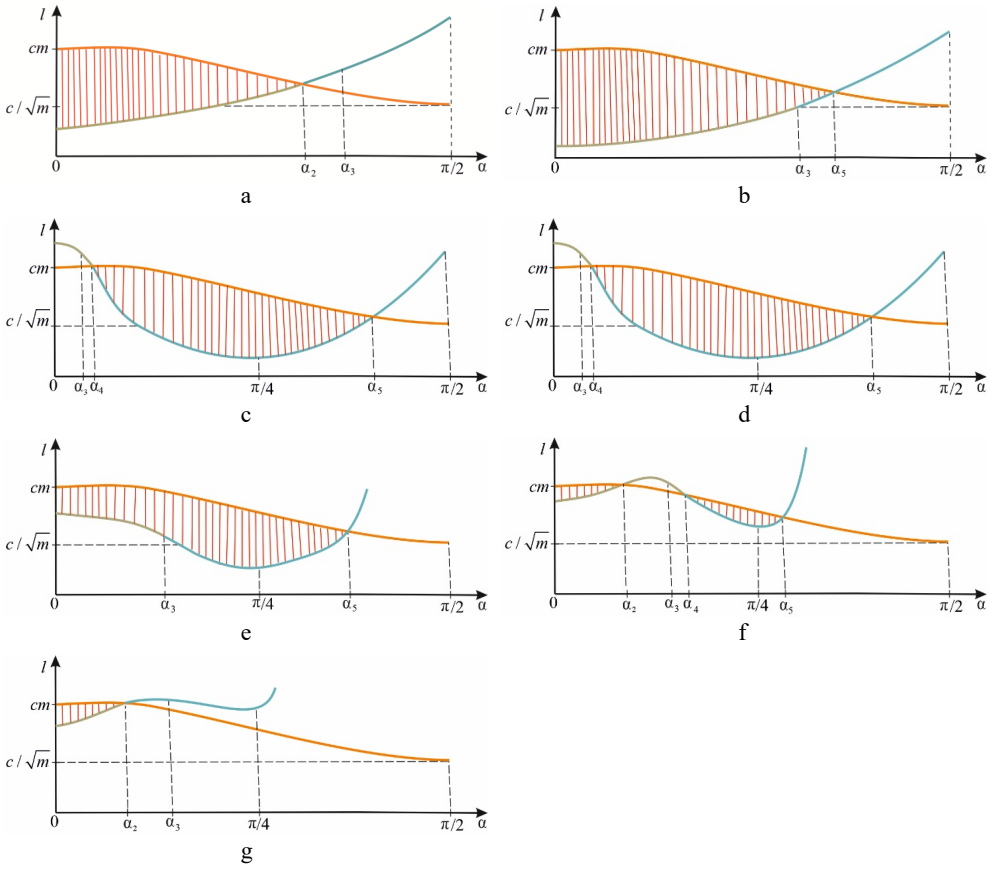

Fig. 3. Region of integration for the function $F_1(P,\eta)$ under compression-tension $(P \le 0, Q \ge 0)$

When $K_{Ic}|\eta|^{-1}(\pi cm)^{-1/2} \le -P < \infty$, we get the region of integration in Figure 3e.

Consider the conditions $-1 < \eta < 0$, $|\eta| \ge \sqrt{(1-\eta)/(1-m^3\eta)}$ and $8\eta^4\left(m^3+1\right)\left(1-\eta^4\right)^{-1} \le 1$. According to the last two inequalities, we will consider the intervals of the change in the value $|P|$. When $2K_{Ic}(1-\eta)^{-1}(\pi cm)^{-1/2}\left(0.5(1+m^3)\right)^{1/4} \le -P \le K_{Ic}|\eta|^{-1}(\pi cm)^{-1/2}$ the region of integration is presented in Figure 3c, for $K_{Ic}|\eta|^{-1}(\pi cm)^{-1/2} \le -P \le K_{Ic}|\eta|^{-1}(\pi cm)^{-1/2}\left(1-m^3\eta\right)^{1/4}(1-\eta)^{-1/4}$ in Figure 3f. The solutions of equation (26) α_4, α_5 on the intervals $(\alpha_3; \pi/4)$ and $(\pi/4; \pi/2)$ can be found here, respectively. We get the region of integration in Figure 3e when $K_{Ic}|\eta|^{-1}(\pi cm)^{-1/2}\left(1-m^3\eta\right)^{1/4}(1-\eta)^{-1/4} \le -P < \infty$.

Consider the case $-1 \le \eta < 0$, $8\eta^4\left(m^3+1\right)\left(1-\eta^4\right)^{-1} \ge 1$. When $K_{Ic}\,|\eta|^{-1}(\pi cm)^{-1/2} \le -P \le 2K_{Ic}(1-\eta)^{-1}(\pi cm)^{-1/2}\left(0.5(1+m^3)\right)^{1/4}$, we get the region of integration in Figure 3g, for $2K_{Ic}(1-\eta)^{-1}(\pi cm)^{-1/2}\left(0.5(1+m^3)\right)^{1/4} \le -P \le K_{Ic}\,|\eta|^{-1}(\pi cm)^{-1/2}\left(1-m^3\eta\right)^{1/4}(1-\eta)^{-1/4}$ in Figure 3f, when $K_{Ic}\,|\eta|^{-1}(\pi cm)^{-1/2}\left(1-m^3\eta\right)^{1/4}(1-\eta)^{-1/4} \le -P < \infty$ in Figure 3b.

After writing down the expressions of the failure loading probability distribution function $F_1\left(|P|,\eta\right)$ according to the obtained areas of integration and substituting the value of the extraction coefficient $m = 1$, we will get the results [15].

5. Probability of failure of plates with extraction

The probability of plate failure with N cracks [15]

$$P_f = F_N(P,\eta) = 1-\left(1-F_1(P,\eta)\right)^N. \tag{27}$$

Based on the obtained expressions, according to (27), it is possible to calculate the probability of failure of a plate with N cracks under different types of stress states, considering the material's technological extraction.

In particular, under uniaxial tension $\left(\eta = 0\right)$

$$P_f = 1-\left(1-\frac{(r+1)\sqrt{m}}{\pi c}\int\limits_{\alpha_1}^{\pi/2}\left[\int\limits_{\frac{K_{Ic}^2}{\pi P^2\sin\alpha}}^{\frac{cm}{\psi(\alpha,m)}}\left(1-\frac{l\psi(\alpha,m)}{mc}\right)^r\psi^{-1}(\alpha,m)\,dl\right]d\alpha\right)^N. \tag{28}$$

Under equibiaxial tension $\left(\eta = 1\right)$

$$P_f = 1-\left(1-\frac{(r+1)\sqrt{m}}{\pi c}\int\limits_{0}^{\alpha_2}\left[\int\limits_{\frac{K_{Ic}^2}{\pi P^2}}^{\frac{cm}{\psi(\alpha,m)}}\left(1-\frac{l\psi(\alpha,m)}{mc}\right)^r\psi^{-1}(\alpha,m)\,dl\right]d\alpha\right)^N. \tag{29}$$

After entering the dimensionless loading $p = P\sqrt{\pi c}/K_{Ic}$ and the value of the cracking parameter $r = 2$, in Figure 4, under expressions (28) and (29), diagrams of the dependence of the probability of failure on the applied loading are presented.

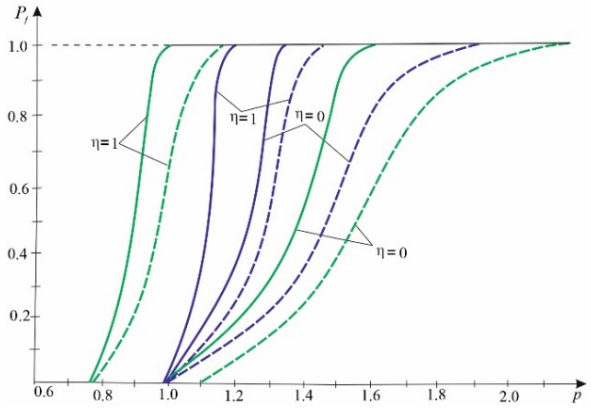

Fig. 4. Probability of failure for some loading cases (solid lines for $N = 100$, dashed for $N = 20$). Purple lines for the plate without extraction, green lines for the plate after extraction ($m = 1.4$)

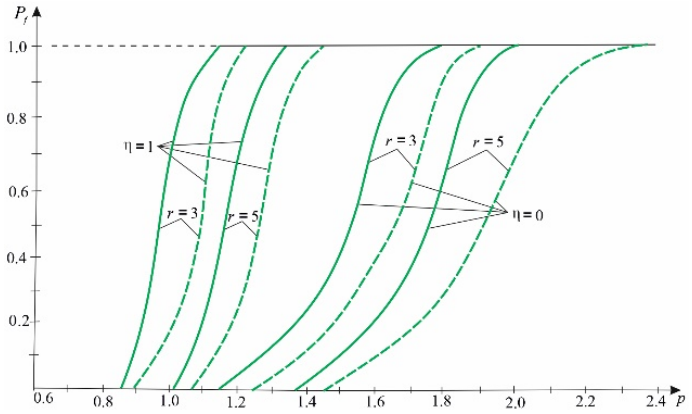

Fig. 5. Probability of failure for different material structural inhomogeneity under different types of stress states

Figure 5 shows the effect on the probability of failure of the structural inhomogeneity of the material and the type of stress state with different numbers of defects in the plate after technological extraction. The designations are similar to Figure 4.

6. Conclusions

According to the graphs in Figure 4, it can be concluded that the previous technological extraction of the plate material led to a decrease in the probability of failure P_f during tension in the direction of the extraction ($\eta = 0$) and an increase in equibiaxial tension ($\eta = 1$). Conversely, the failure loading corresponding to the specified probability of failure P_f increases due to processing during tension

in the extraction direction and decreases with equibiaxial tension. As the number of cracks in the plate increases, the failure loading corresponding to the fixed probability of failure decreases, and the probability of failure increases.

Under a fixed-loading P, with an increase in the parameter r (the structure of the plate material becomes homogeneous), we get a pattern of decreasing probability of failure (Fig. 5). This regularity depends on the stress state type. Similar regularities were observed in the article [24].

The conducted research makes it possible to estimate and predict the strength and strength anisotropy of stochastically defective structural elements under a complex stress state, depending on the coefficient of technological extraction, considering the number of defects.

References

[1] Sabirov, I., M., Perez-Prado, M., Molina-Aldareguia, J., Semenova, I., Salimgareeva, G., & Valiev, R. (2011). Anisotropy of mechanical properties in high-strength ultra-fine-grained pure Ti processed via a complex severe plastic deformation route. *Scripta Materialia*, *64*(1), 69-72. DOI: 10.1016/j.scriptamat.2010.09.006.

[2] Chen, T., Lu, H.Z., Lin, J.A., Cai, W.S., Zhu, D.Z., & Yang. C. (2023). Tailoring microstructure and mechanical properties of CP-Ti through combined treatment of pressure and pulsed electric current. *Journal of Materials Research and Technology*, 25, 3496-3506. DOI: 10.1016/ j.jmrt.2023.06.147.

[3] Bažant, Z., & Chen, E.P. (1997). Scaling of structural failure. *Applied Mechanics Reviews*, *50*(10), 593-627. DOI: 10.1115/1.3101672.

[4] Chowdhury, M.S., Song, C., & Gao, W. (2014). Probabilistic fracture mechanics with uncertainty in crack size and orientation using the scaled boundary finite element method. *Composite Structures*, *137*, 93-103. DOI: 10.1016/j.compstruc.2013.03.002.

[5] Lei, W.S. (2016). Fracture probability of a randomly oriented microcrack under multi-axial loading for the normal tensile stress criterion. *Theoretical and Applied Fracture Mechanics*, *85*(B), 164-172. DOI: 10.1016/j.tafmec.2016.01.004.

[6] Choi, W., Yoon, S., & Lee L.J. (2017). Crack simulation and probability analysis using irregular truss structure modeling equivalent to a continuum structure. *International Journal of Agricultural and Biological Engineering*, *10*(1), 234-247. DOI: 10.3965/j.ijabe.20171001.2024.

[7] Gao, X., Koval, G., & Chazallon, C. (2017). Energetical formulation of size effect law for quasi-brittle fracture. *Engineering Fracture Mechanics*, *175*(15), 279-292. DOI: 10.1016/ j.engfracmech.2017.02.001.

[8] Lei, W.-S. (2018). A generalized weakest-link model for size effect on strength of quasi-brittle materials. *Journal of Materials Science*, *53*(2), 1227-1245.

[9] Rakesh, P., More, A., Kumar, M., & Muthu, N. (2022). Probabilistic failure prediction in a double composite cantilever beam with single and double source uncertainty. *Composite Structures*, *279*, 114870. DOI: 10.1016/j. compstruct.2021.114870.

[10] Kumar, R., Madsen, B., Lilholt, H., & Mikkelsen, L. (2022). Influence of test specimen geometry on probability of failure of composites based on Weibull weakest link theory. *Materials*, *15*(11), 3911. DOI: 10.3390/ma15113911.

[11] Wan, L., Ullah, Z., Yang, D., & Falzon, B.G. (2023). Probability embedded failure prediction of unidirectional composites under biaxial loadings combining machine learning and micromechanical modeling. *Composite Structures*, *312*, 116837. DOI: 10.1016/j.compstruct.2023.

[12] Pagnoncelli, A.P., Paolino D.S., Peroni, L., & Tridello, A. (2024). Innovative tensile test for brittle materials: Validation on graphite R4550. *International Journal of Mechanical Sciences*, *261*, 108679. DOI: 10.1016/j.ijmecsci.2023.108679.

[13] Alabdullah, M., & Ghoniem N.M. (2024). A probabilistic-phase field model for the fracture of brittle materials. *Modelling and Simulation in Materials Science and Engineering*, *32*(1), 015002. DOI: 10.1088/1361-651X/ad09ea.

[14] Vera, J., Caballero Garcia, L.F., Taboada Neira, M., & Valverde Flores J.F. (2024). Probability of defects detection in welded joints using the magnetic particle method. *Archives of Metallurgy and Materials*, *69*(2), 607-612. DOI: 10.24425/amm.2024.149789.

[15] Vitvits'kii, P., & Popina, S. (1980). Strength and Criteria of Brittle Fracture of Stochastically Defective Bodies. Kyiv, 186.

[16] Hahn, G., & Shapiro, S. (1994). *Statistical Models in Engineering*, 376. ISBN-13: 978047104 0651.

[17] Vitvits'kii, P., & Kvit, R. (1992). Probabilistic description of experimental statistical strength characteristics. *Soviet Materials Science*, *28*(1), 83-86. DOI: 10.1007/BF00723637.

[18] Li, X., Konietzky, H., Li, X., & Wang, Y. (2019). Failure pattern of brittle rock governed by initial microcrack characteristics. *Acta Geotechnica*, *14*(5), 1437-1457. DOI: 10.1007/s11440--018-0743-5.

[19] Romanovsky, V. (1979). *Reference Book on Cold Forming.* Mechanical Engineering.

[20] Korolyuk, V., Skorokhod, A., Portenko, N., & Turbin, A. (1985). *A Manual on Probability Theory and Mathematical Statistics.* Nauka.

[21] Kvit, R. (2023). Development of the statistical model failure of orthotropic composite materials. *Journal of Applied Mathematics and Computational Mechanics*, *22*(2), 26-35. DOI: 10.17512/ jamcm.2023.2.03.

[22] Kvit, R. (2022). Investigation of probabilistic aspects reliability of isotropic bodies with internal defects. *Journal of Applied Mathematics and Computational Mechanics*, *21*(3), 73-84. DOI: 10.17512/jamcm.2022.3.06.

[23] Mossakovskii, V., & Rybka, M. (1965). An attempt to construct a theory of fracture for brittle materials, based on Griffith's criterion. *Journal of Applied Mathematics and Mechanics*, *29*(2), 326-332. DOI: 10.1016/0021-8928(65)90034-1.

[24] Pukach, P., Kvit, R., Salo, T., & Vovk, M. (2023). A probable approach to reliability assessment of reinforced plates. *Applied System Innovation*, *6*(4), 73. DOI: 10.3390/asi6040073.